engineering proceedings

MDPI

Proceeding Paper

Position-Aware Neural Precoding Using Physics-Based Ray-Tracing Channels †

Pin-Chih Lin and Jake W. Liu *

Department of Electronic Engineering, National Taipei University of Technology, Taipei 10608, Taiwan
* Correspondence: jwliu@ntut.edu.tw
† Presented at the 6th International Conference on Electronic Communications, Internet of Things and Big Data (ICEIB 2026), New Taipei, Taiwan, 24–26 April 2026.

Abstract

A location-aided neural precoding scheme is proposed for millimeter-wave beamforming, where a multilayer perceptron maps receiver coordinates directly to a unit-norm complex beamforming vector, replacing instantaneous channel state information (CSI). Physics-based ray-tracing channels are generated exclusively offline for training. Evaluations in the Sionna Ray Tracer Munich scenario at 28 GHz with an 8-element uniform linear array show that the learned precoder achieves 95.5% of the matched-filter upper bound, outperforming a 16-point oversampled Discrete Fourier Transform codebook (90.4%) without beam sweeping. The network implicitly captures scene geometry, forming side lobes aligned with dominant non-line-of-sight reflections. Performance is maintained under localization errors up to 2.0 m standard deviation, demonstrating the viability of coordinate-driven, scene-aware beamforming as a low-latency alternative to CSI-based methods.

Keywords: millimeter-wave (mmWave) communications; beamforming; precoding; deep learning; location-aided communication; ray tracing; codebook-based beam training; Sionna RT

1. Introduction

Millimeter-wave (mmWave) systems rely on highly directional beamforming to compensate for severe pathloss and blockages [1]. The viability of mmWave mobile communications has been extensively validated in early studies [2]. In current 5G New Radio deployments [3–5], beam alignment is typically achieved via discrete codebooks and exhaustive sweeping, introducing substantial latency. Moreover, the finite angular resolution of practical codebooks causes scalloping loss [6], significantly degrading performance for users located between quantized beam directions. This raises a fundamental question: can spatial side information, such as user coordinates, directly infer near-optimal beamforming weights without real-time CSI acquisition or exhaustive scanning? Various location-aided approaches, including orientation-aware beam selection [7], have been explored to address this.

Ray tracing (RT) provides a deterministic, physics-driven channel model capturing realistic multipath propagation and geometric scattering. RT-based simulators are increasingly adopted to generate rich channel datasets for deep learning [8,9], while environment-aware hybrid precoding strategies [10] have been combined with such data. Location-conditioned neural networks further minimize beam-training overhead in highly mobile environments [11].

Check for updates

Academic Editors: Teen-Hang Meen, Shu-Han Liao and Cheng-Fu Yang

Published: 27 October 2026

Copyright: © 2026 by the authors. Licensee MDPI, Basel, Switzerland. This article is an open access article distributed under the terms and conditions of the Creative Commons Attribution (CC BY) license.

In this paper, we utilize the Sionna Ray Tracer (RT) module version 2.0.1 [12,13] (built upon Mitsuba [14]) to synthesize realistic narrowband multiple-input single-output channels. We propose a neural precoder parameterized by a multilayer perceptron (MLP) that directly maps continuous receiver coordinates to unit-norm complex beamforming weights, drawing on deep-learning-based physical layer design [15,16]. RT is used offline as a physics-based channel generator; gradients are computed solely with respect to the precoder parameters, investigating whether spatial coordinates suffice to learn a near-optimal, scene-aware beamformer.

The proposed precoder enables a lightweight MLP to map 3D coordinates to unit-norm beamforming weights without real-time CSI and continuous spatial coverage that eliminates scalloping loss, achieving 95.5% of the MRT bound. The physics-based evidence indicates that the network implicitly exploits non-line-of-sight reflections, showing robustness to positioning noise up to $\sigma = 2.0$ m.

2. Formulation

2.1. System Model

We modeled a wireless downlink communication system consisting of a fixed base station (BS) equipped with a uniform linear array (ULA) of N_{tx} antennas with half-wavelength spacing, and a mobile user equipment (UE) with a single antenna. Let $\mathbf{p} = [x, y, z]^{\text{T}} \in \mathbb{R}^3$ denote the 3D spatial coordinates of UE. The narrowband channel vector at carrier frequency f_{c} is denoted as:

$$\mathbf{h}(\mathbf{p}) \in \mathbb{C}^{N_{\text{tx}} \times 1}. \tag{1}$$

Here, $\mathbf{h}(\mathbf{p})$ is determined by the deterministic physical wave propagation (including line-of-sight and geometric multipath reflections) obtained via a ray-tracing (RT) engine based on the 3D scene geometry and the transceivers' locations. The transmitted signal after precoding is given by:

$$\mathbf{x} = \mathbf{w}s, \tag{2}$$

Here, $s \in \mathbb{C}$ is the transmitted data symbol (with $\mathbb{E}\left[|s|^2\right] = 1$), and $\mathbf{w} \in \mathbb{C}^{N_{\text{tx}} \times 1}$ is the unit-norm precoding vector (beamformer) satisfying $\|\mathbf{w}\|_2 = 1$. The signal received at the UE located at $\mathbf{p}$ is formulated as:

$$y = \mathbf{h}(\mathbf{p})^{\text{H}}\mathbf{w}s + n, \tag{3}$$

Here, $n \sim \mathcal{CN}(0, \sigma_{\text{n}}^2)$ is the additive white Gaussian noise (AWGN), and $(\cdot)^{\text{H}}$ denotes the Hermitian (conjugate transpose) operator. The effective received signal power (excluding noise) for a given location $\mathbf{p}$ and precoder $\mathbf{w}$ is:

$$P(\mathbf{p}, \mathbf{w}) = \left|\mathbf{h}(\mathbf{p})^{\text{H}}\mathbf{w}\right|^2. \tag{4}$$

Coordinate-to-beam mapping is conducted by maximizing the outcome of Equation (4) without real-time channel estimation.

2.2. Precoding Methods

2.2.1. MRT

Assuming perfect channel state information (CSI), the matched-filter precoder is given as Equation (5), which maximizes the received power $\left|\mathbf{h}^{\text{H}}\mathbf{w}\right|^2$ under the unit-norm constraint, serving as the performance upper bound.

$$\mathbf{w}_{\text{MRT}} = \frac{\mathbf{h}}{\|\mathbf{h}\|_2}, \tag{5}$$

https://doi.org/10.3390/engproc2026159033

2.2.2. Discrete Fourier Transform (DFT) Codebook

The baseline DFT codebook $\mathbf{W} \in \mathbb{C}^{N_{\text{tx}} \times K}$ with $K = 16$ beams has (n, k)-th element:

$$[\mathbf{W}]_{n,k} = \frac{1}{\sqrt{N_{\text{tx}}}} e^{j2\pi \frac{nk}{K}} \tag{6}$$

Here, $n \in \{0, \ldots, N_{\text{tx}} - 1\}$. Hierarchical codebook designs [17] can speed up beam training. The selected codeword via exhaustive beam sweeping is:

$$\mathrm{w}^{\text{JB}} = \arg\max_{\mathrm{k}} |\mathrm{h}^{\mathrm{H}} \mathrm{w}_{\mathrm{k}}|^2 \mathbf{w}_{\text{CB}} = \arg\max_{k} |\mathbf{h}^{\mathrm{H}} \mathbf{w}_k|^2 \tag{7}$$

2.2.3. Proposed Neural Precoder

The proposed neural precoder is MLP parameterized by θ, which directly maps the normalized receiver position to complex precoding weights:

$$\mathbf{w}_{\text{NN}} = f_\theta(\tilde{\mathbf{p}}),\ \tilde{\mathbf{p}} = (\mathbf{p} - \boldsymbol{\mu}) \oslash \boldsymbol{\sigma} \tag{8}$$

Here, $\boldsymbol{\mu}$, $\boldsymbol{\sigma}$ are the empirical position statistics, and $\oslash$ is element-wise division. The MLP outputs a $2N_{\text{tx}}$-dimensional real vector split into real/imaginary parts, yielding a unit-norm complex vector via:

$$f_\theta(\tilde{\mathbf{p}}) = \frac{\mathbf{a}_{\text{out}} + j\mathbf{b}_{\text{out}}}{\|\mathbf{a}_{\text{out}} + j\mathbf{b}_{\text{out}}\|_2} \tag{9}$$

2.3. Training Objective

The precoder is trained by minimizing the expected negative received power:

$$\min_\theta \mathcal{L}(\theta) = -\mathbb{E}_{\mathbf{p} \in \mathcal{D}} \left[|\mathbf{h}(\mathbf{p})^{\mathrm{H}} f_\theta(\tilde{\mathbf{p}})|^2 \right] + \lambda \|\theta\|_2^2 \tag{10}$$

Here, $\mathcal{D}$ is the training location dataset, and λ is the L_2 weight decay coefficient.

2.4. Ray-Tracing-Based Channel Generation

To obtain physically realistic and spatially consistent channel vectors without relying on stochastic models, we employ a deterministic ray-tracing engine:

$$\mathbf{h}(\mathbf{p}) = \mathrm{RT}(\mathbf{p}, \text{scene}) \tag{11}$$

Here, $\mathrm{RT}(\cdot)$ simulates the narrowband channel via the coherent summation of deterministic propagation paths—including line-of-sight (LoS), specular reflections, and refractions—traced from the known 3D environmental geometry. The ray-tracing computation is executed strictly offline; channel realizations $\mathbf{h}(\mathbf{p})$ are cached as fixed environmental ground truths and excluded from the computational graph. Gradients are computed solely with respect to the neural precoder parameters θ via the chain rule:

$$\frac{\partial \mathcal{L}}{\partial \theta} = \left(\frac{\partial \mathcal{L}}{\partial \mathbf{w}_{\text{NN}}} \right) \left(\frac{\partial \mathbf{w}_{\text{NN}}}{\partial \theta} \right) \tag{12}$$

This design bypasses channel derivatives with respect to position or scene parameters ($\partial \mathbf{h} / \partial \mathbf{p}$ is not computed), ensuring a lightweight training process focused on learning a robust coordinate-to-beam mapping.

https://doi.org/10.3390/engproc2026159033

2.5. Performance Metric

We evaluate all methods by the MRT efficiency η, i.e., the normalized received power ratio:

$$\eta_{\mathrm{NN}} = \frac{P_{\mathrm{NN}}}{P_{\mathrm{MRT}}} = \frac{|\mathbf{h}^{\mathrm{H}}\mathbf{w}_{\mathrm{NN}}|^2}{|\mathbf{h}^{\mathrm{H}}\mathbf{w}_{\mathrm{MRT}}|^2} \tag{13}$$

Similarly, $\eta_{\mathrm{CB}} = P_{\mathrm{CB}}/P_{\mathrm{MRT}}$ for the codebook; $\eta \to 1$ indicates near-optimal matched-filter performance.

3. Result

3.1. Evaluation of Average Performance

We evaluate the single-link 1-transmit/1-receive multiple-input single-output channel system in the realistic Sionna RT Munich environment at $f_c = 28$ GHz. BS is equipped with an $N_{\mathrm{tx}} = 8$ ULA with half-wavelength spacing. Receiver locations are uniformly sampled in a rectangular street grid ($x \in [30, 55]$ m, $y \in [60, 95]$ m, $z = 1.5$ m), generating 8192 channel realizations split into 70% training and 30% validation sets. Ray tracing is configured with a maximum depth of 5, incorporating LoS, specular reflections, and refractions. To isolate beam-alignment quality from large-scale pathloss, we apply standard crest factor reduction normalization such that $\mathbb{E}\left[\|\mathbf{h}\|_2^2\right] \approx N_{\mathrm{tx}}$. This ensures that the average MRT received power equals N_{tx}, enabling fair cross-method comparison. Table 1 summarizes the key parameters.

Table 1. Settings for numerical evaluation.

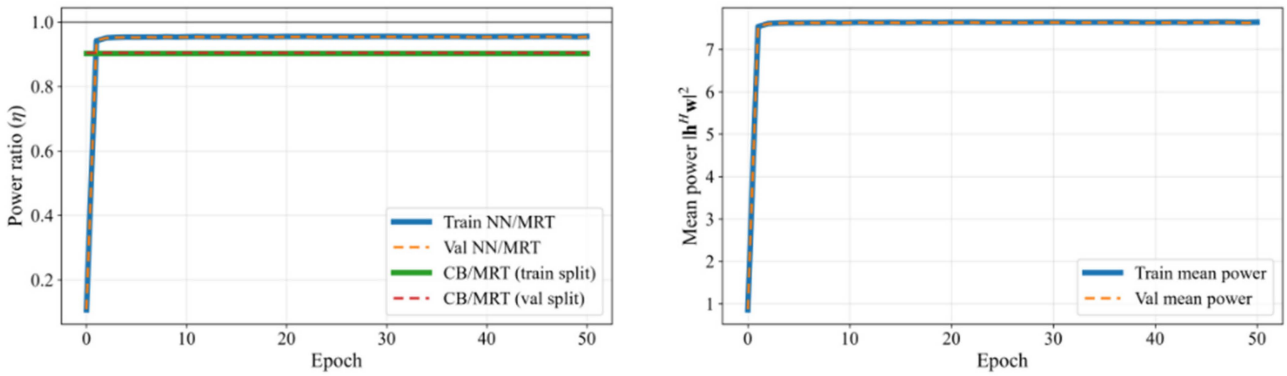
Setting	Value
Scene	Sionna RT Munich
Carrier frequency	28 GHz
Transmit array	ULA, $N_{\mathrm{tx}} = 8$, spacing 0.5λ
Receive array	Single antenna
Receiver region	$x \in [30, 55]$ m, $y \in [60, 95]$ m, $z = 1.5$ m
Ray tracing	depth 5, LoS + specular + refraction, diffuse off
Dataset	8192 samples, 70/30 train/val split
Neural precoder	MLP (3×128 ReLU), unit-norm output
Optimizer	Adam, lr 2×10^{-3}, batch 128, epochs 50
Codebook baseline	DFT, $K = 16$ (oversampled)

Figure 1 shows the learning curves. MLP converges rapidly within the first 10 epochs, stabilizing at $\eta = 0.955$. The close alignment between training and validation curves confirms generalization without overfitting.

Table 2 summarizes the average precoding performance. At initialization (epoch 0), the untrained MLP behaves as a random beamformer, capturing only 10.9% of the MRT bound. After 50 epochs of training, the proposed neural precoder successfully learns the position-to-beam mapping, achieving an MRT efficiency of $\eta_{\mathrm{NN}} = 0.955$. This effectively outperforms the strong oversampled 16-point DFT codebook baseline ($\eta_{\mathrm{CB}} = 0.904$), while eliminating the significant latency required for 16 over-the-air beam sweeps.

To translate these power gains into practical link-level metrics, we configure the noise variance such that the average MRT signal-to-noise ratio (SNR) is 10 dB ($\mathbb{E}[P_{\mathrm{MRT}}]/\sigma_{\mathrm{n}}^2 = 10$). Using the analytical quadrature phase-shift keying bit error rate approximation in additive white Gaussian noise (BER $\approx$ Q($\sqrt{\mathrm{SNR}}$)), the oversampled codebook yields a mean BER of 1.3×10^{-3}, whereas the proposed neural precoder reduces the mean BER to 1.0×10^{-3} (closely approaching the MRT theoretical limit of 7.8×10^{-4}).

https://doi.org/10.3390/engproc2026159033



(**a**) (**b**)

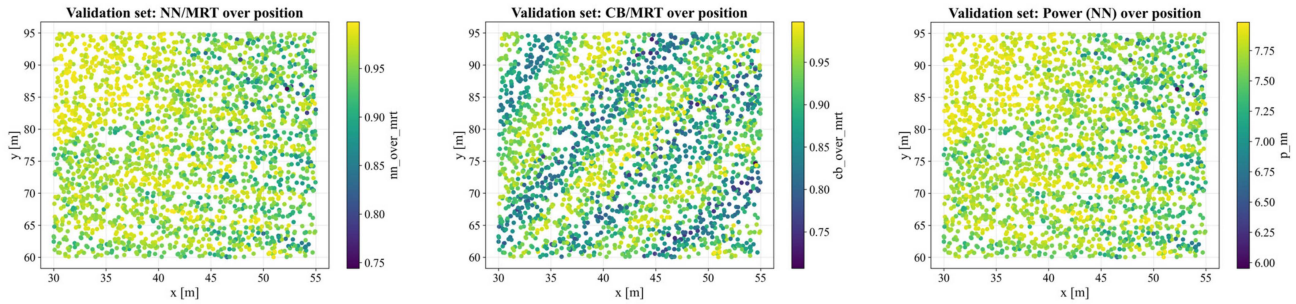
Figure 1. Learning curves showing rapid convergence and generalization. The neural precoder stabilizes at $\eta = 0.955$, surpassing the 16-point DFT codebook ($\eta = 0.904$). (**a**) Power ratios (η); (**b**) Mean received power.

Table 2. Validation results (mean over 2458 unseen locations).

Method	Mean P	MRT Efficiency (η)	Gain vs. Codebook Baseline
NN (epoch 0)	0.868	0.109	0.120×
DFT Codebook ($K = 16$)	7.235	0.904	1.000×
Proposed NN (epoch 50)	7.636	0.955	1.055×
MRT (Upper Bound)	8.000	1.000	1.106×

3.2. Spatial Coverage and Scalloping Loss Mitigation

Beyond average metrics, the spatial distribution of the performance ratio highlights the fundamental advantage of the proposed continuous mapping paradigm. As visualized in the spatial heatmaps in Figure 2, the performance of the two approaches differs drastically depending on the user coordinates. Even a highly dense 16-point DFT codebook exhibits localized scalloping loss, manifesting as dark spots (often $\eta < 0.8$) when users are located in the coverage gaps between fixed quantized beam directions [Figure 2b].



(**a**) NN/MRT (epoch 50) (**b**) CB/MRT (**c**) P under NN (epoch 50)

Figure 2. Spatial performance over receiver locations (validation split): (**a**) The neural precoder yields consistently high ratios across the region. (**b**) Despite using a dense 16-point dictionary, the DFT codebook degrades in locations where departure angles are misaligned with fixed beams. (**c**) Absolute received power under the trained neural precoder varies across the region due to local propagation conditions.

In contrast, Figure 2a shows that the neural precoder provides universally robust coverage. By dynamically synthesizing optimal, continuous phase weights tailored to exact

coordinates, the MLP effectively eliminates the discrete beam boundaries. The heatmap is dominated by high-efficiency regions (yellow/light green), smoothly bridging the physical spaces that discrete dictionaries struggle to serve. Finally, Figure 2c shows the absolute received power P_{NN}, visualizing how the trained model seamlessly adapts to local propagation conditions and multipath richness across the complex urban geometry.

3.3. Physics-Based Interpretability and Scene Geometry

A fundamental question regarding location-based beamforming is whether the neural network simply memorizes the geometric line-of-sight (LoS) direction to the receiver, or if it genuinely learns to exploit the complex wave propagation environment. To investigate this, we visualize the spatial radiation pattern [normalized array gain versus angle of departure (AoD)] synthesized by the proposed neural precoder for a specific test location characterized by strong multipath reflections.

As depicted in Figure 3, the main lobe of the neural precoder (blue solid line) closely matches that of the theoretical MRT upper bound (green dashed line). More importantly, the ray-tracing engine identifies distinct non-line-of-sight reflections (NLoS) multipath components (MPCs) at specific angles (approximately +30° and +57°, marked by red dotted lines). Without explicit CSI during inference, the neural precoder automatically forms side lobes that precisely align with these reflection paths. This provides physics-based evidence that the MLP implicitly internalizes the 3D scene geometry and steers energy toward structural scatterers to constructively combine at the receiver.

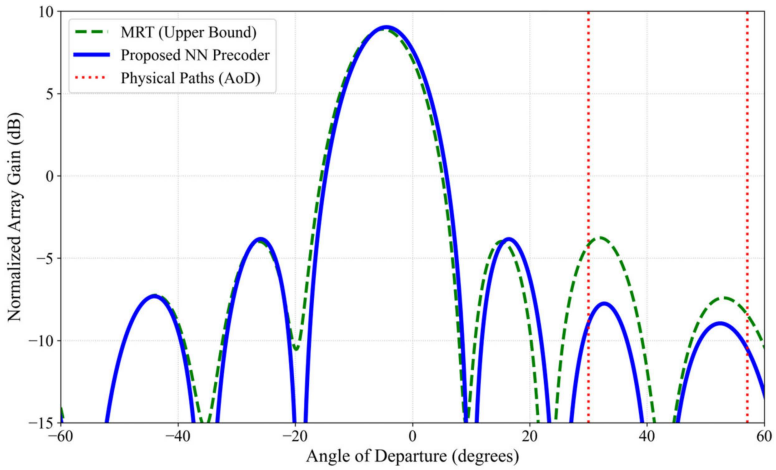


Figure 3. Spatial radiation pattern of the learned neural precoder compared to the optimal MRT beamformer for a selected test location. The red dotted lines indicate the ground-truth physical AoD of the dominant MPCs obtained from the ray tracer.

3.4. Robustness to Positioning Errors

A critical challenge in deploying location-aided beamforming systems is the inevitable inaccuracy of practical localization mechanisms such as the Global Navigation Satellite System or vision-based tracking in complex urban environments. To rigorously evaluate the practical resilience of the proposed method, we perform a sensitivity analysis by injecting isotropic zero-mean Gaussian noise $\mathcal{N}(0, \sigma^2)$ into the horizontal spatial coordinates (x, y) of the unseen validation set during the inference phase, simulating realistic coordinate drifts. Recent empirical studies highlighted that GPS errors in real-world urban canyons significantly impact beam prediction accuracy [18].

As illustrated in Figure 4, the proposed neural precoder demonstrates strong robustness against spatial uncertainty. For typical localization errors ($\sigma \leq 1.0$ m), performance

degradation is minimal ($\eta \geq 0.945$), indicating the MLP learned a smooth spatial mapping rather than overfitting to exact coordinates. The neural precoder maintains a clear advantage over the 16-point DFT codebook ($\eta_{\mathrm{CB}} = 0.904$) for positioning errors up to $\sigma \approx 2.0$ m, without incurring any beam-sweeping latency. Even under extreme localization failures ($\sigma = 5.0$ m), the model retains acceptable functionality ($\eta = 0.779$), validating the reliability of the scene-aware mapping for real-world mmWave deployments.

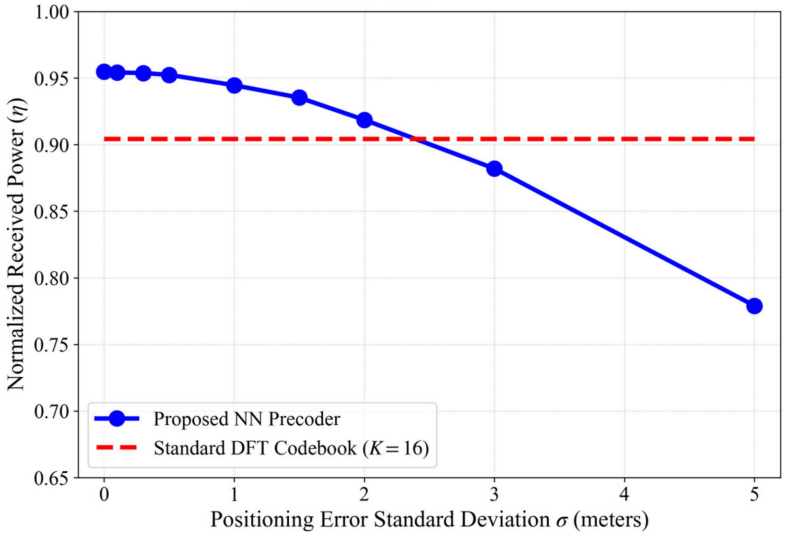


Figure 4. Sensitivity analysis of the precoding performance under localization uncertainty. The proposed neural precoder maintains superior normalized received power compared to the standard codebook under realistic positioning noise ($\sigma \leq 2.0$ m).

4. Conclusions

Spatial coordinates can serve as an effective surrogate for instantaneous CSI in millimeter-wave beamforming, provided that scene-consistent channel data is available for offline learning. By leveraging deterministic ray-tracing channels, the proposed neural precoder learns a smooth coordinate-to-beam mapping that achieves 95.5% of the matched-filter upper bound, effectively eliminating the scalloping loss inherent to discrete beam steering. Crucially, the approach consistently outperforms a dense 16-point DFT codebook (90.4%) without incurring any exhaustive beam sweeping overhead. Beyond performance gains, radiation pattern analysis confirms that the learned mapping remains physically consistent with the underlying propagation geometry, implicitly synthesizing side lobes to exploit NLoS multipath reflections. The observed robustness to localization errors further supports the practical deployment feasibility, demonstrating superiority over exhaustive scanning under realistic positioning noise (up to $\sigma = 2.0$ m). Future extensions are required to include wideband channels, hybrid architectures, multi-user precoding, and joint optimization with differentiable ray-tracing environments.

Author Contributions: Conceptualization, J.W.L.; methodology, P.-C.L. and J.W.L.; software, P.-C.L.; validation, P.-C.L.; formal analysis, P.-C.L. and J.W.L.; writing—original draft preparation, P.-C.L.; writing—review and editing, J.W.L.; supervision, J.W.L. All authors have read and agreed to the published version of the manuscript.

Funding: This research received no external funding.

Institutional Review Board Statement: Not applicable.

Informed Consent Statement: Not applicable.

Data Availability Statement: The simulation data used in this study are available from the corresponding author upon reasonable request.

Conflicts of Interest: The authors declare no conflicts of interest.

References

1. Heath, R.W.; Gonzalez-Prelcic, N.; Rangan, S.; Roh, W.; Sayeed, A.M. An overview of signal processing techniques for millimeter wave MIMO systems. *IEEE J. Sel. Top. Signal Process.* **2016**, *10*, 436–453. [CrossRef]
2. Rappaport, T.S.; Sun, S.; Mayzus, R.; Zhao, H.; Azar, Y.; Wang, K.; Wong, G.N.; Schulz, J.K.; Samimi, M.; Gutierrez, F. Millimeter wave mobile communications for 5G cellular: It will work! *IEEE Access* **2013**, *1*, 335–349. [CrossRef]
3. Morais, D.H. 5G NR overview and physical layer. In *Key 5G/5G-Advanced Physical Layer Technologies*; Springer: Cham, Switzerland, 2024; pp. 233–321.
4. Lagen, S.; Wanuga, K.; Elkotby, H.; Goyal, S.; Patriciello, N.; Giupponi, L. New radio physical layer abstraction for system-level simulations of 5G networks. In Proceedings of the ICC 2020-2020 IEEE International Conference on Communications (ICC), Dublin, Ireland, 7–11 June 2020; pp. 1–7.
5. Giordani, M.; Polese, M.; Roy, A.; Castor, D.; Zorzi, M. A tutorial on beam management for 3GPP NR at mmWave frequencies. *IEEE Commun. Surv. Tuts.* **2019**, *21*, 173–196. [CrossRef]
6. Hur, S.; Kim, T.; Love, D.J.; Krogmeier, J.V.; Thomas, T.A.; Ghosh, A. Millimeter wave beamforming for wireless backhaul and access in small cell networks. *IEEE Trans. Commun.* **2013**, *61*, 4391–4403. [CrossRef]
7. Rezaie, S.; De Carvalho, E.; Manchón, C.N. A deep learning approach to location- and orientation-aided 3D beam selection for mmWave communications. *IEEE Trans. Wirel. Commun.* **2022**, *21*, 11110–11124. [CrossRef]
8. Alkhateeb, A. DeepMIMO: A generic deep learning dataset for millimeter wave and massive MIMO applications. *arXiv* **2019**, arXiv:1902.06435.
9. Wu, D.; Zeng, Y.; Jin, S.; Zhang, R. Environment-aware and training-free beam alignment for mmWave massive MIMO via channel knowledge map. In Proceedings of the 2021 IEEE International Conference on Communications Workshops (ICC Workshops), Montreal, QC, Canada, 14–23 June 2021; pp. 1–7.
10. Alkhateeb, A.; El Ayach, O.; Leus, G.; Heath, R.W. Channel estimation and hybrid precoding for millimeter wave cellular systems. *IEEE J. Sel. Top. Signal Process.* **2014**, *8*, 831–846. [CrossRef]
11. Alkhateeb, A.; Alex, S.; Varkey, P.; Li, Y.; Qu, Q.; Tujkovic, D. Deep learning coordinated beamforming for highly-mobile millimeter wave systems. *IEEE Access* **2018**, *6*, 37328–37348. [CrossRef]
12. Hoydis, J.; Cammerer, S.; Aoudia, F.A.; Vem, A.; Binder, N.; Marcus, G.; Keller, A. Sionna: An open-source library for next-generation physical layer research. *arXiv* **2022**, arXiv:2203.11854.
13. Aoudia, F.A.; Hoydis, J.; Nimier-David, M.; Nicolet, B.; Cammerer, S.; Keller, A. Sionna RT: Technical report. *arXiv* **2025**, arXiv:2504.21719.
14. Nimier-David, M.; Vicini, D.; Zeltner, T.; Jakob, W. Mitsuba 2: A retargetable forward and inverse renderer. *ACM Trans. Graph.* **2019**, *38*, 1–17.
15. O'Shea, T.; Hoydis, J. An introduction to deep learning for the physical layer. *IEEE Trans. Cogn. Commun. Netw.* **2017**, *3*, 563–575. [CrossRef]
16. Chege, J.K.; Yeredor, A.; Haardt, M. Probabilistic position-aided beam selection for mmWave MIMO systems. In Proceedings of the 33rd European Signal Processing Conference (EUSIPCO 2025), Palermo, Italy, 8–12 September 2025; pp. 2107–2111. [CrossRef]
17. Xiao, Z.; He, T.; Xia, P.; Xia, X.-G. Hierarchical codebook design for beamforming training in millimeter-wave communication. *IEEE Trans. Wirel. Commun.* **2016**, *15*, 3380–3392. [CrossRef]
18. Morais, J.; Bchboodi, A.; Pezeshki, H.; Alkhateeb, A. Position-aided beam prediction in the real world: How useful GPS locations actually are? In Proceedings of the ICC 2023-IEEE International Conference on Communications, Rome, Italy, 28 May–1 June 2023; pp. 1824–1829.

Disclaimer/Publisher's Note: The statements, opinions and data contained in all publications are solely those of the individual author(s) and contributor(s) and not of MDPI and/or the editor(s). MDPI and/or the editor(s) disclaim responsibility for any injury to people or property resulting from any ideas, methods, instructions or products referred to in the content.